NV Diamond Magnetometry

Nicolas Scozzaro

Candidacy Exam

The Ohio State University

January 8, 2013

Abstract

Recent progress in confocal fluorescence microscopy techniques has enabled optical excitation and read out of single nitrogen vacancy (NV) centers in diamond. The NV center is a spin-1 system that is one of many defects common to diamond, but it is unique in that it fluoresces at a different rate depending on its spin state, giving the experimentalist a way to read out the spin state in nearly real time. Furthermore, the spin state can be manipulated using optical pumping techniques in which a cycle of transitions is driven based on whether an applied microwave (RF) signal is on resonance with either the ground state $|0\rangle \rightarrow |+1\rangle$ or $|0\rangle \rightarrow |-1\rangle$ transitions. And, since the $|+1\rangle$ and $|-1\rangle$ states experience changes in energy based on the magnetic field applied along the NV axis, this consequently changes the corresponding RF resonance frequency, yielding a direct relationship between applied field and resonance frequency. Thus the NV center can be used not simply as a magnetometer, but a vector magnetometer since it is only the component of field along the NV axis that changes the resonance condition. In recent experiments by Yacoby et al. [6, 17], they use the information provided by such spin-state dependent fluorescence and resonance-dependent fluorescence to demonstrate both AC and DC scanning magnetometry using a single NV centers as the sensor. In this paper I will discuss the theory and methods behind these novel experiments, and compare their results to other related techniques to highlight the significance of their work.

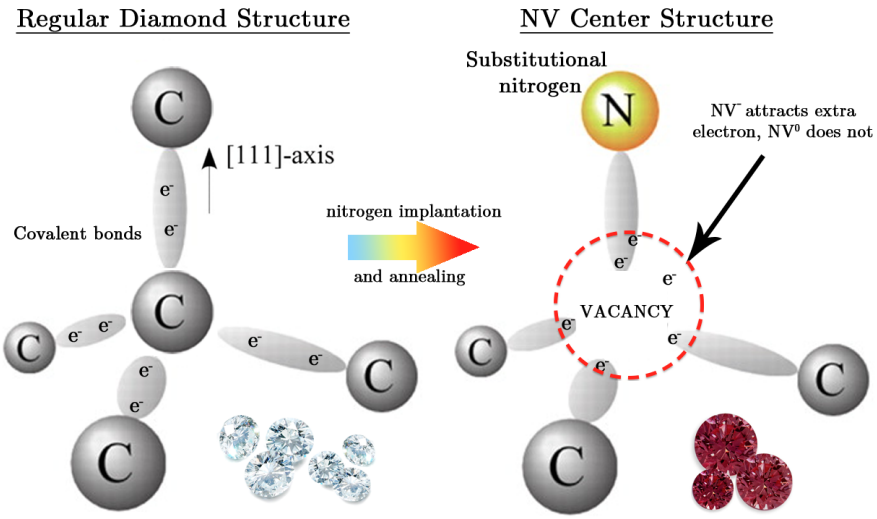

Figure 1.1: The main "caltrop" tetrahedral building block of the diamond lattice consists of 5 carbon atoms that form covalent bonds with its four nearest neighbors. An NV center is formed by substituting one carbon with a nitrogen atom and removing an adjacent carbon, leaving a vacancy.

1 NV Diamond Structure

Diamonds are probably best known for their aesthetics, with the 4 C's of "Cut, Clarity, Color, and Carat" setting the deep blue sparkling, cushion-cut Hope diamond apart from ordinary stones. The 4 C's are due to interesting physics that happen uniquely in diamonds: the first C, the cut, gives rise to the 'brilliance' which is made possible due to diamond's high index of refraction: clever cutting angles causes light to fully internally reflect, making diamonds sparkle in a way that no other gem can. But it's the middle two C's, clarity and color, due to defects and impurities, that give rise to the key physics that are the topic of this paper.

Pure diamond has a large band gap of 5.4 eV, which means that only photons with energies corresponding to ultraviolet light or higher can be absorbed; photons of optical energy and below pass straight through (or get reflected at the surfaces) making a pure diamond appear transparent. However, if some of the carbon atoms on the tetrahedral diamond lattice are replaced with nitrogen or boron atoms, or removed altogether leaving vacancies, this will add states with energies in the band gap. This allows the diamond to absorb and emit photons with lower energies, in the optical range

and into the infrared, as well as providing new avenues for creating phonons and adding vibrational energy to the lattice. The exact physics of these effects, like the dynamic Jahn-teller effect, crystal distortions and photon-phonon interactions, is not the central topic of this paper but may be further explored in other references [2, 6]. These effects cause nitrogen-doped diamond to absorb blue light and fluoresce yellow, and boron-doped diamonds to absorb ultraviolet and fluoresce blue; in fact, the latter is one of the ways that jewelers verify that a stone is in fact a diamond. Yet it is not the standard substitutional nitrogen center called a P1 center, but the substitutional nitrogen paired with a vacant lattice site called a "nitrogen-vacancy center" (NV center) that is the focus here.

Let's explore the NV center structure. A carbon atom has 6 electrons, and when placed on a lattice the 4 valence electrons make covalent bonds with 4 neighboring atoms on a tetrahedral lattice to make diamond. Nitrogen atoms have 7 electrons, one more than carbon, and when they are shot at a pure diamond they will knock carbon atoms out of the way until they settle into place — usually interstitially, but sometimes substitutionally [16]. There will be vacancies left in the tracks of the nitrogen, and by annealing the diamond, putting it in a furnace in temperatures upwards of 950 °C (˜1750 °F), the carbon atoms will jostle around and eliminate most of the vacancies; however, some vacancies will move around and pair up next to a nitrogen, forming a nitrogen vacancy center as depicted in figure 1.1. A further treatment involving irradiation of the diamond with electrons creates more vacancies and has been found to increase the number of NV centers, but is not always necessary [6, 16]. The center can be neutral (NV^0) with 5 electrons, 3 from the carbon atoms and two from the nitrogen atom; or it can be negatively charged (NV^-) with 6 electrons, the same five electrons as NV^0, but with one additional electron.

The NV^- center is used almost exclusively in magnetic resonance experiments because it shows a strong EPR signal compared to NV^0 [17], but its energy levels are non-trivial. The 6 electrons end up making a composite spin-1 boson, which has certain symmetries that determine its allowed energy levels. These symmetries are best understood and derived using group theory, making linear combinations of molecular orbitals, but even then some of the essential details of the electronic structure have been ascertained experimentally [16]. The essential features of the energy levels that are used experimentally are:

- A ground state consisting of 3 levels: $m_s \in -1,\ 0,\ 1$ (a triplet state called ${}^3A_2$)
- An excited state consisting of 3 levels: $m_s \in -1,\ 0,\ 1$ (a triplet state called ${}^3E$)
- States in between the ground state and excited state: $m_s = 0$ (singlet and xy-orbital called ${}^1E$ and ${}^1A_1$, often referred to as 'metastable' because they are longer lived than the excited states)

If we focus on just the Hamiltonian for the ground states, we have [5]

$$\mathcal{H} = \underbrace{DS_z^2 + E\left(S_x^2 - S_y^2\right)}_{\substack{\text{crystal field} \\ \text{(zero-field) splitting}}} + \underbrace{g_e\mu_B\vec{B}\cdot\vec{S}}_{\substack{\text{electron} \\ \text{Zeeman}}} + \underbrace{A_\parallel S_z I_z + A_\perp\left(S_x I_x + S_y I_y\right)}_{\substack{\text{hyperfine coupling to} \\ \text{nitrogen nucleus}}} + \underbrace{PI_z^2}_{\substack{\text{quad-} \\ \text{rupole}}} - \underbrace{g_N\mu_N\vec{B}\cdot\vec{S}}_{\substack{\text{nuclear} \\ \text{Zeeman}}}, \quad (1.1)$$

where the terms have been grouped in order of magnitude, largest first within the range $1\,\text{G} \lesssim B \lesssim 1000\,\text{G}$ (since for zero field the Zeeman term vanishes, while for fields larger than ~1000 G there is the level crossing of the $|-1\rangle$ and $|0\rangle$ states). For small fields the zero-field splitting term dominates, and since $D \gg E$ (ie. the axial ZFS is much greater than the transverse ZFS) we have the effective ground state Hamiltonian:

$$\mathcal{H}_{\mathcal{GS}} \approx DS_z^2 + g_e\mu_B\vec{B}\cdot\vec{S}, \quad (1.2)$$

where $D = 2.87$ GHz is the zero-field splitting constant, g_e is the electron g-factor, μ_B is the Bohr magneton, B is the applied magnetic field, and S is the spin of the NV center. Note that this Hamiltonian does *not* describe all the energy levels as one may conventionally be used to seeing, but only the ground-state energy levels; the excited and metastable states are obtained through other methods of analysis as previously noted.

2 Optical Pumping of the NV Center

The techniques of optical pumping were originally developed in the 1950's in seminal work by Alfred Kastler, for which he received the Nobel prize, and very similar techniques are used to this day to manipulate NV centers. Kastler worked with rubidium gases, and discovered that the atoms can be optically excited, then selectively driven in a cycle depending on whether an additional RF signal is

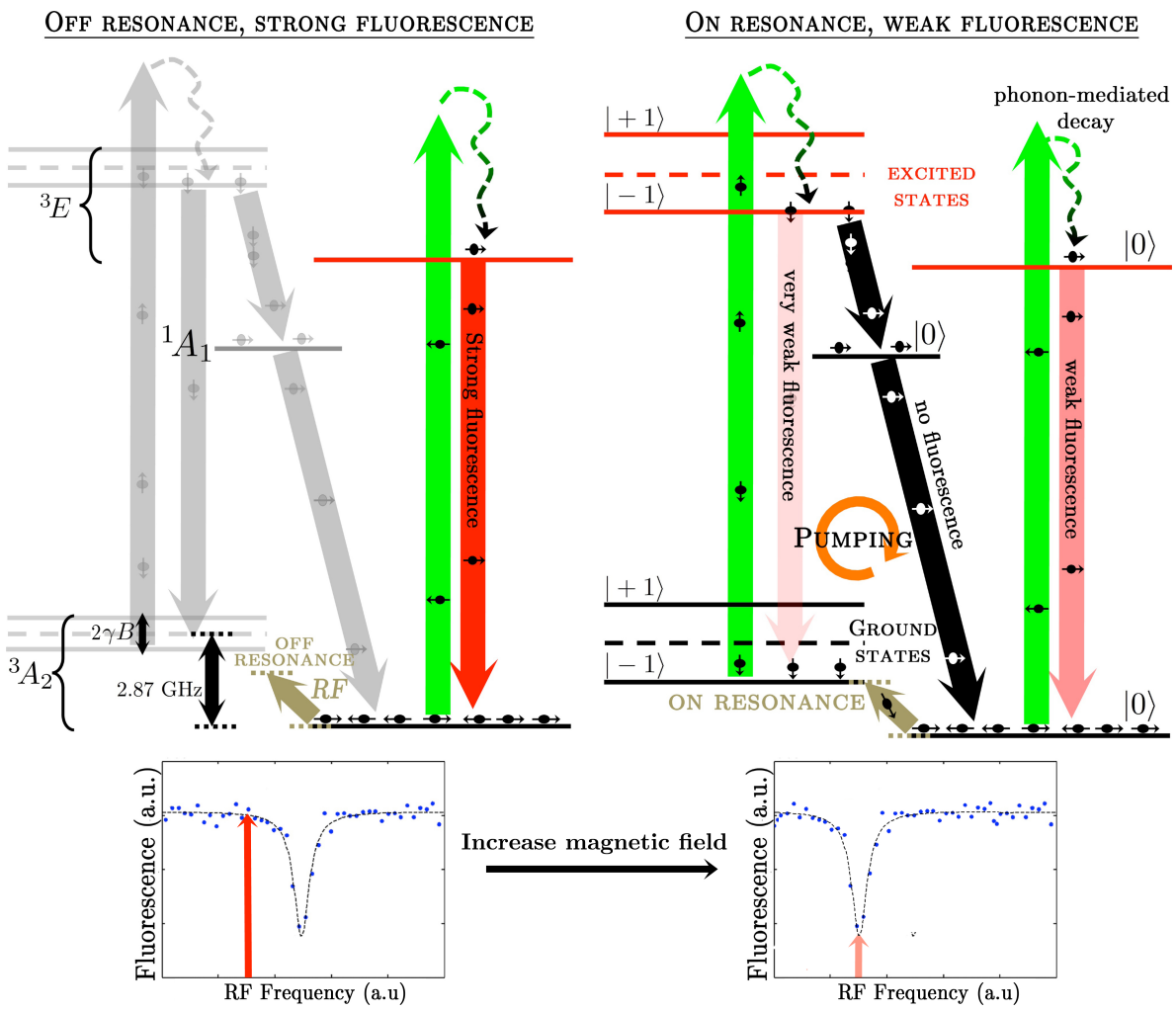

Figure 2.1: An RF signal is depicted as initially tuned below resonance with the $|-1\rangle$ state (the $|+1\rangle$ state can be used as well), and the system is not pumping as represented by the greyed-out states and transitions; the spins are excited by green light from the ground $|0\rangle$ state, have a phonon-mediated decay to the excited $|0\rangle$ state, then fluoresce red strongly as they decay to the ground state. As the magnetic field is increased, the $|-1\rangle$ state comes on resonance with the RF and a significant number of spins are continuously 'pumped': they're cyclically excited from the $|0\rangle$ to $|-1\rangle$ state, then are excited by green light, and finally decay without fluorescence through the singlet or with very weak fluorescence back to the $|-1\rangle$ state. This causes the overall fluorescence to decrease when on resonance. Note that the ^1E state is not pictured here, as its role in non-fluorescent decay is not entirely understood.

applied on resonance with one of rubidium's allowed ground state transitions. When the RF is not applied, the atoms absorb incident light and get 'optically pumped' up a ladder of states until reaching the top rung, at which point by selection rules the light cannot be absorbed any more. But, if RF is applied, it kicks the pumped atoms back down to the bottom of the ladder, enabling them to climb back up, absorbing light en route. The gas is placed in between a light source and a photodetector, so when the RF is off the light *is not* absorbed and the photodetector receives a strong signal, and when the RF is on the light *is* absorbed and the photodetector receives a weaker signal. Let's compare this to common optical pumping techniques with NV centers.

For NV center optical pumping it is not the excitation light itself, but the fluorescence induced by the excitation light that yields the signal that is detected. But, just like with rubidium, a weaker signal is detected when the RF is on resonance than off resonance. In zero magnetic field, the NV center's $|+1\rangle$ and $|-1\rangle$ states are degenerate, with a splitting of 2.87 GHz from the $|0\rangle$ state (see figure 2.1). When a magnetic field B is applied along the NV axis, it breaks the degeneracy, raising the $|+1\rangle$ state and lowering the $|-1\rangle$ state by an amount γB. Whereas in zero field the NV center is resonated by RF at 2.87 GHz, in a magnetic field it is resonated by RF at the Larmor frequency [1]

$$f_{|0\rangle\rightarrow|\pm1\rangle} = 2.87 \text{ GHz} \pm \gamma B, \tag{2.1}$$

where $\gamma = 28$ GHz/T is the gyromagnetic ratio for the NV center spin (which happens to be the same value as for an isolated electron spin). Since B is the only unknown in determining the resonance condition, this yields a method for determining the magnitude and direction of the magnetic field (along the NV axis); thus magnetometry with NV centers is inherently vector magnetometry[2].

[1] Note that the units of γ can be expressed in terms of either angular frequency $\frac{\text{rad}}{\text{s}\cdot\text{T}}$, or frequency $\frac{1}{\text{s}\cdot\text{T}}$ ($\frac{\text{Hz}}{\text{T}}$), with the values of 1.76×10^{11} $\frac{\text{rad}}{\text{s}\cdot\text{T}}$ or $28\frac{\text{GHz}}{\text{T}} = 2.8\frac{\text{MHz}}{\text{G}}$, respectively.

[2] Note that while a magnetic field transverse to the NV axis does not cause Zeeman splitting, it can induce mixing between states that can cause changes in fluorescence.

3 DC Magnetometry

In recent experiments by Yacoby et al. [6, 17], they apply an external field B and use the resonance corresponding to the $|0\rangle \rightarrow |-1\rangle$ transition to do magnetometry, $f_{|0\rangle\rightarrow|-1\rangle} = 2.87 \text{ GHz} - \gamma B$. They monitor the fluorescence on both sides of the Lorentzian fluorescence signal as in figure 3.1, detuned by an amount equal to the linewidth $\pm\Gamma$, where $\Gamma = 6.62$ MHz $\Leftrightarrow$ 2.4 G — they alternatively used a detuning of 10 MHz when a larger magnetic field range was required (but with less sensitivity). As they scan a single NV center over a magnetic surface (in a manner similar to magnetic force microscopy), small changes in magnetic field due to magnetic features shift the resonance frequency, so the fluorescence on one side of the dip increases as the fluorescence on the other side decreases. The ESR fluorescence signal $I(f, B)$ can be experimentally fit to a Lorentzian,

$$I(f,B) = C_0 - (C_0 - C_1)\,\frac{\left(\frac{\Gamma}{2}\right)^2}{\left[f - f_0\,(B)\right]^2 + \left(\frac{\Gamma}{2}\right)^2}, \tag{3.1}$$

where C_0 is the off-resonance fluorescence, C_1 is the on-resonance fluorescence, Γ is the linewidth (full width at half max), f is the applied RF frequency, and $f_0(B)$ is the resonance frequency which is a function of the magnetic field. If we detune f from resonance by the linewidth such that $f = f_0\,(B_0) \pm \Gamma$, and have small changes in magnetic field such that $f_0\,(B) = f_0\,(B_0) \pm \gamma\delta B$, we have[3]

$$\delta I(\delta B) = C_0 - (C_0 - C_1)\,\frac{\left(\frac{\Gamma}{2}\right)^2}{\left[\left(f_0\,(B_0) \pm \Gamma\right) - \left(f_0\,(B_0) + \gamma\delta B\right)\right]^2 + \left(\frac{\Gamma}{2}\right)^2},$$

$$\Rightarrow \delta I = C_0 - (C_0 - C_1)\,\frac{\left(\frac{\Gamma}{2}\right)^2}{\left[\pm\Gamma - \gamma\delta B\right]^2 + \left(\frac{\Gamma}{2}\right)^2} \approx \mp\frac{(C_0 - C_1)}{\Gamma}\,(\gamma\delta B)\,. \tag{3.2}$$

Equation (3.2) simply says that if we choose a positive detuning ($+\Gamma$), an increase in magnetic field $+\delta B$ will bring the NV center closer to resonance and decrease the fluorescence, and the converse for a negative detuning.

In these experiments both a hard drive and a magnetic dipole were used as the magnetic samples of

[3] The expansion of $\delta I(\delta B)$ for small δB given in equation (3.2) can be obtained either by hand, or in *Mathematica* using the command: Series $\left[\text{c0} - \frac{\left(\frac{\Gamma}{2}\right)^2(\text{c0}-\text{c1})}{(\Gamma-\gamma\delta\text{B})^2+\left(\frac{\Gamma}{2}\right)^2}, \{\delta\text{B}, 0, 1\}\right]$

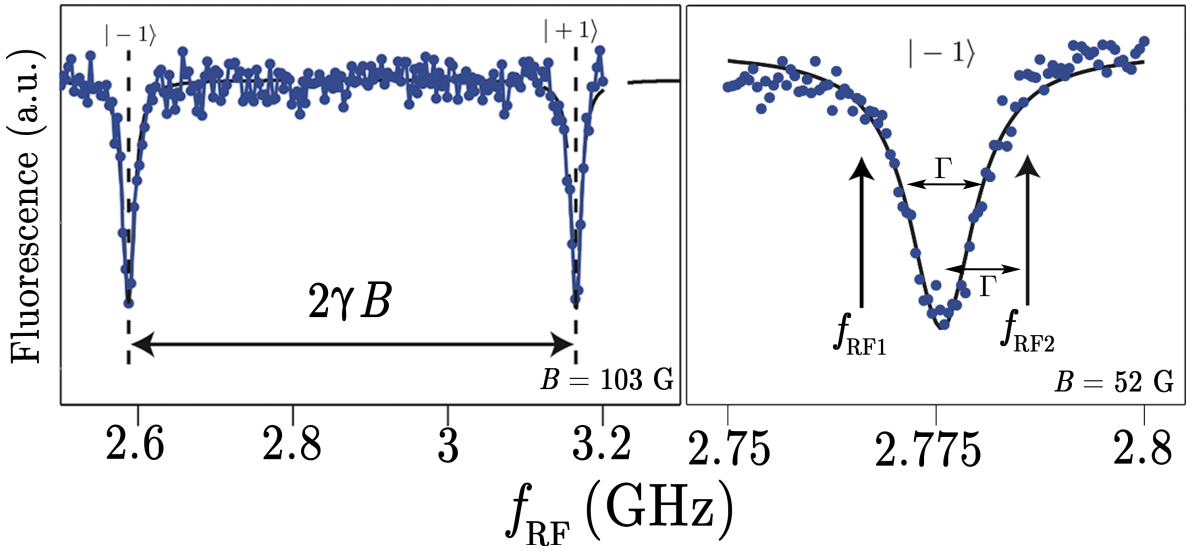

Figure 3.1: Left, the ESR spectrum for a single NV center obtained by sweeping the RF frequency through the $|0\rangle \rightarrow |-1\rangle$ and $|0\rangle \rightarrow |+1\rangle$ transitions of the $^3A_2$ states in an applied field of $B = 103$ G. The resonance frequencies are given by equation 2.1. Right, in DC magnetometry experiments by Yacoby et al., they chose the $|0\rangle \rightarrow |-1\rangle$ transition in an applied field of $B = 52$ G, and monitored the fluorescence at frequencies corresponding to the linewidth $\pm\Gamma$ above and below resonance as the NV was scanned over a hard drive.

study. In the hard drive study, magnetic domains (representing bits) were oriented out-of-plane with magnitudes of roughly ± 3 G; however, at the domain walls between neighboring bits, there were strong transverse fields which undesirably suppressed fluorescence, decreasing the contrast of the magnetic field images.

4 AC Magnetometry

A more sophisticated magnetometry technique performed by Yacoby et al. called 'AC magnetometry' involves modulating the spatial separation between the magnetic sample of interest and an NV center while monitoring the NV center's phase accumulation. In the experiment, the sample is taken to be a magnetic coating on a tuning fork resonator, similar to the magnetic coating commonly sputtered on cantilevers for use in magnetic force microscopy. The magnetic material forms a roughly dipolar magnetic field, and as the tuning fork oscillates, it causes the magnitude and direction of the magnetic

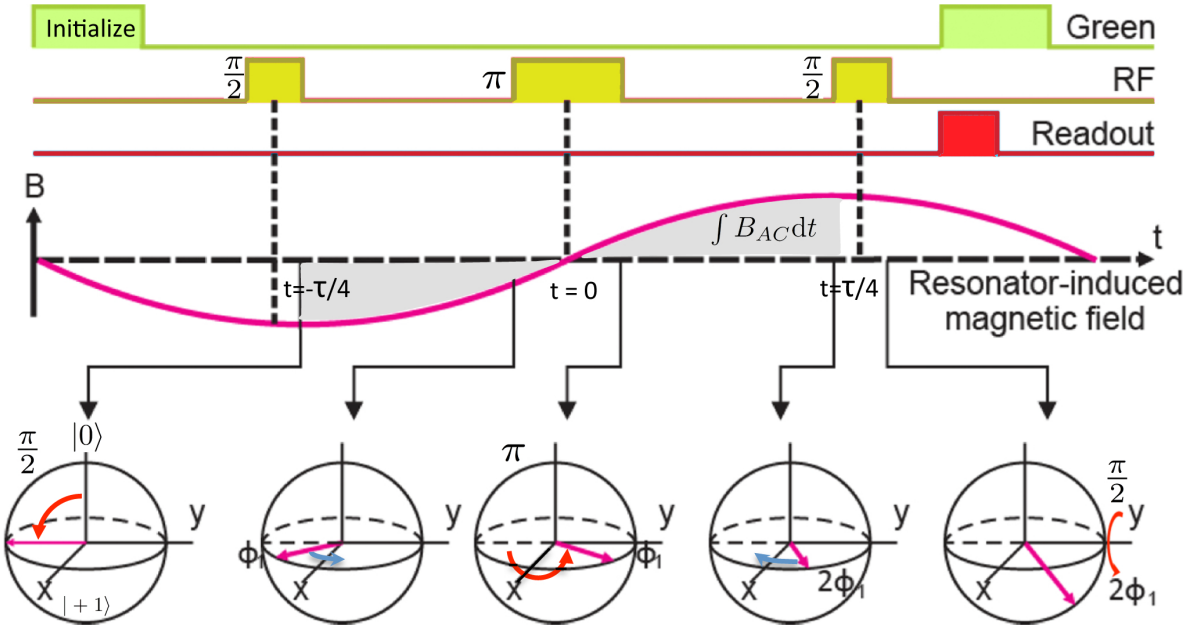

Figure 4.1: Protocol for AC magnetometry spin manipulation with accompanying Bloch spheres. The NV spin is initialized in the $|0\rangle$ state by green light. A $\frac{\pi}{2}$ pulse then brings the spin into the x-y plane at which point it starts to accumulate phase due to AC (oscillator-induced) magnetic field, with the phase proportional to the left shaded region. This is followed by a π-pulse and more phase accumulation. The phase is then projected onto the z-axis by a final $\frac{\pi}{2}$ pulse, and read out by application of green light. Note that the pulses are not shown to scale and are actually very short relative to the oscillator frequency.

field at the location of the NV center to vary. The NV center was oriented along the $[0, \sqrt{2}, 1]$ axis, while the magnetic moment was oriented along the $[0, 0, 1]$ axis. Since the NV center's levels are only split by the component of the magnetic field along the NV-axis, to get the total field along the NV axis we must take the dot product of the tuning fork oscillator's dipolar magnetic field, $\mathbf{B}_{dip}$, with the NV center's (unit vector) axis $\hat{\mathbf{n}}$,

$$B(x, y, z, t) = B_0 + \underbrace{\mathbf{B}_{dip}(x, y, z, t) \cdot \hat{\mathbf{n}}}_{\equiv \delta B(t)}, \tag{4.1}$$

where B_0 is the external field, and x, y, and z are the position of the NV center with respect to the oscillator. In the experiment, the oscillator has small amplitude oscillations δx (20 nm) along the x-

axis, so $\delta B(t)$ can be approximated as a time independent component $\mathbf{B}_{dip}(x,y,z)\cdot\hat{\mathbf{n}} \equiv B_{dip}(x,y,z)$, plus a time-dependent sinusoidal sampling of the field at a nearby point $(x+\delta x, y, z)$,

$$\delta B(t) = B_{dip}(x,y,z) + \frac{\partial B_{dip}(x,y,z)}{\partial x}\delta x \sin(2\pi f_{osc} t), \tag{4.2}$$

where f_{osc} is the oscillator's frequency, and $\frac{\partial B_{dip}(x,y,z)}{\partial x} \equiv G_{nv_x}$ is the x-component of the dipolar field gradient along the NV axis. Thus the total magnetic field is the sum of a DC field, $B_{DC} = B_0 + B_{dip}$, and an AC field, $B_{AC}(t) = G_{nv_x}\delta x \sin(2\pi f_{osc} t)$. In DC magnetometry, there is no oscillation of the sample and consequently there is no AC component to the magnetic field — one simply normalizes their fluorescence to B_0 and monitors the changes in fluorescence due to the sample's position-dependent magnetization (in this case $B_{dip}(x,y,z)$). On the other hand, in AC magnetometry a Hahn-echo like series of RF pulses causes the phase accumulated due to the DC component to cancel out, leaving only the effects due to the AC component.

The system is first initialized by applying green light in the absence of an RF signal, pumping the NV center into the ground $|0\rangle$ state. An RF pulse is then applied on resonance with the $|0\rangle$ to $|+1\rangle$ transition (as given by equation (2.1)) . When the pulse is applied, the spin starts to Rabi-precess at a frequency determined by the strength of the field generated by the RF coil, in this case $H_1 = H_{RF} = 4.46$ G $\Leftrightarrow 6.25$ MHz $\equiv \Omega_{Rabi}$. Rabi precession causes the expectation value of the spin to oscillate sinusoidally from the initialized state, $|0\rangle$, to a superposition of $|0\rangle$ and $|+1\rangle$, to purely the $|+1\rangle$ state, then back again; on the Bloch sphere, this is represented by the spin's expectation value being oriented along the z-axis, x-y plane, and $-z$-axis respectively, as in figure 4.1. Once initialized, an RF $\frac{\pi}{2}$-pulse along the $-x$-axis causes the spin to Rabi precess onto the $-y$-axis of the Bloch sphere, timed such that the sinusoidal AC magnetic field is near a minimum. At this point the spin starts to accumulate phase due to the magnetic field for a time $t = \frac{\tau}{4}$, where $\tau \approx \frac{1}{f_{osc}}$ is approximately the period of the oscillator (but need not be exactly). During this time the DC magnetic field is oriented along the z-axis, which causes the spin to gain an amount of phase $\phi_0 = (2\pi \times 2.87\text{ GHz} + \gamma B_{DC})\frac{\tau}{4}$ (not shown in figure 4.2), whereas the AC magnetic field causes the spin to accumulate an amount of

phase (with respect to the $-y$-axis) given by

$$\phi_1 = \int_{\frac{-\tau}{4}}^{0} \gamma B_{AC}(t)\mathrm{d}t = \int_{\frac{-\tau}{4}}^{0} \gamma \left[G_{nv_x}\delta x \sin\left(2\pi f_{osc}t\right)\right]\mathrm{d}t = \frac{\gamma G_{nv_x}\delta x}{2\pi f_{osc}}\left[\cos\left(2\pi f_{osc}\frac{\tau}{4}\right) - 1\right]. \tag{4.3}$$

Experimentally all parameters are known except for the gradient G_{nv_x}, thus by measuring ϕ_1 we can map the x-component of the gradient of the field along the NV axis (that's a mouthful!).

After the quarter period of phase accumulation the spin is π-pulsed (at $t = 0$), resulting in a phase of $\pi - (\phi_0 + \phi_1)$, still with respect to the $-y$-axis. The spin then continues to accumulate more phase for another quarter period: the DC field again causes the spin to accumulate a phase $+\phi_0$, while the AC field switches sign, for a total phase of $[\pi - (\phi_0 + \phi_1)] + \phi_0 - \phi_1 = \pi - 2\phi_1$; note that the phase due to the DC field has been canceled by these pulses. A final $\frac{\pi}{2}$-pulse about the y-axis projects this phase back onto the z-axis, followed by green laser light for optical readout of the spin state. If P is the probability of being in a state, the correspondence between the final spin state and the phase is given by the expression

$$P_{|0\rangle} = \frac{1 - \sin\left(2\phi_1\right)}{2}, \qquad P_{|+1\rangle} = 1 - P_{|0\rangle} = \frac{1 + \sin\left(2\phi_1\right)}{2}, \tag{4.4}$$

which is measured as a fluorescence signal,

$$I(\phi_1) = I_{avg} - I_{pk}\sin\left(2\phi_1\right). \tag{4.5}$$

This is simply a statement that when the spin is in the pure $|0\rangle$ state $\left(2\phi_1 = \frac{3\pi}{2}\right)$ there is maximum fluorescence, $I_{avg} + I_{pk}$, when it's in an equal superposition of $|0\rangle$ and $|+1\rangle$ $(2\phi_1 = 0, \pi)$ there is an average fluorescence, I_{avg}, and when it's in the pure $|+1\rangle$ state $\left(2\phi_1 = \frac{\pi}{2}\right)$ there is minimum fluorescence, $I_{avg} - I_{pk}$. Combining equations 4.3 and 4.5, we have

$$\begin{aligned} I\left(\phi_1\right) &= I_{avg} - I_{pk}\sin\left(2\frac{\gamma G_{nv_x}\delta x}{2\pi f_{osc}}\left[\cos\left(2\pi f_{osc}\frac{\tau}{4}\right) - 1\right]\right) \\ &\Rightarrow I(x,y) \approx I_{avg} + I_{pk}\sin\left(\frac{\gamma\delta x}{\pi f_{osc}}G_{nv_x}(x,y)\right), \end{aligned} \tag{4.6}$$

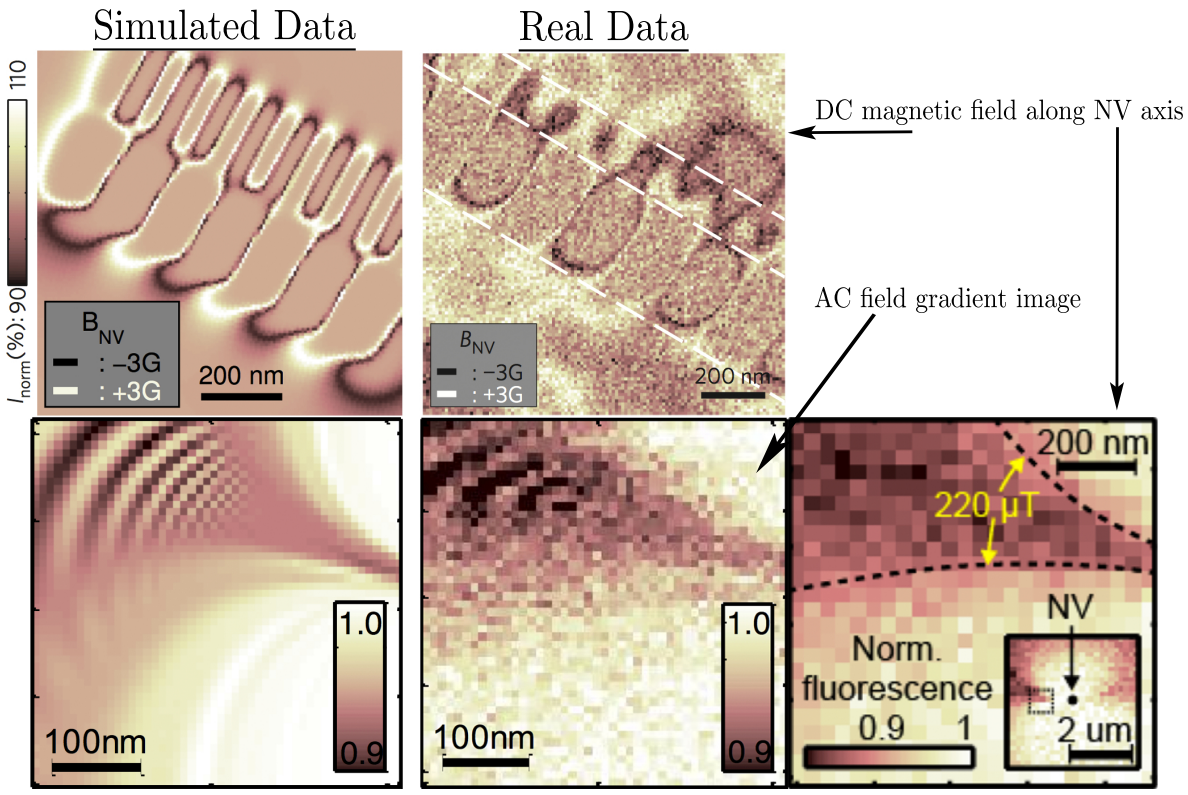

Figure 4.2: DC and AC magnetometry images. The top two images are simulated and measured data for scanning DC magnetometry on a hard drive: an NV center is scanned 70 nm above the surface of the hard drive in the presence of a uniform 52 G external field. As the NV is scanned, the components of magnetic field along the NV axis due to the hard drive cause the fluorescence to dim for negative fields and brighten for positive fields: the scale bar, I_{norm}, is described in the DC magnetometry section, and the inset of ±3 G is a conversion of the fluorescence to field. The bottom left two images are the simulated and measured AC field gradient data for a fixed NV center, around which a magnetic dipole is scanned; the data is described by equation (4.6). The last image is also a DC field image, and the inset shows a zoomed-out scan in which the dipolar nature of the gradient is easily recognized. Note that the similarity between the AC image gradient image and the DC field image is coincidental.

where in the last line the fluorescence is expressed in terms of position to highlight that equation (4.6) is used to create the fluorescence map as in figure 4.2. Note that the fluorescence signal changes from max to min when the argument of sine changes by π, which corresponds to a change in the gradient of: $\frac{\gamma\delta x}{\pi f_{osc}}\Delta G_{nv_x}(x,y) = \pi \Rightarrow \Delta G_{nv_x}(x,y) \approx 0.01\frac{\mathrm{G}}{\mathrm{nm}} = 1\frac{\mu\mathrm{T}}{\mathrm{nm}}$. Thus a gradient that changes quickly as a function of position (or at least by more than $0.01\frac{\mathrm{G}}{\mathrm{nm}}$) manifests itself as a series of dark and bright bands as in the top left corner of figure 4.2.

5 Sensitivity

The sensitivity of both AC and DC magnetometry is ultimately limited by photon shot noise. Shot noise arises because the NV center emits photons with a Poisson distribution in time, so sometimes the photons arrive at the photodetector in bursts, and sometimes they arrive more spread out compared to a steady stream of photons. It is the average number of counts per unit time (the fluorescence rate) which contains the information of the spin state, so if the fluorescence is monitored for too short a period of time it's possible to catch a burst of photons which would erroneously yield a fluorescence rate higher than the actual average. As the NV center is scanned there are changes in magnetic field that correspondingly cause changes in the fluorescence rate; thus it is the ability to distinguish fluorescence rates that ultimately limits the magnetic field sensitivity.

Two fluorescence rates can be distinguished given that the rates differ by more than the noise, and the noise in the fluorescence rate I is given by $\sigma_I = \sqrt{I}$ according to Poisson statistics. In DC magnetometry the fluorescence is measured on the sides of the Lorentzian resonance dip, so the average fluorescence is about half the on-resonance and off-resonance fluorescence rates, $\langle I\rangle = \frac{C_0+C_1}{2}$ from equation (3.1). The uncertainty in the fluorescence rate is then

$$\sigma_I = \sqrt{\frac{C_0 + C_1}{2}},$$

yet it's the uncertainty in the B field, σ_B that we're after. The two are related by $\sigma_I = \frac{\partial I}{\partial B}\sigma_B$, and since the change in the fluorescence for a change in magnetic field is given by $\frac{\delta I}{\delta B} = \frac{\partial I}{\partial B} = \frac{\gamma(C_0-C_1)}{\Gamma}$ from equation (3.1), we have the noise limit for DC magnetometry,

$$\sigma_{B_{DC}} = \frac{\sqrt{\frac{C_0+C_1}{2}}}{\frac{\gamma(C_0-C_1)}{\Gamma}} \approx 14\frac{\mu\text{T}}{\sqrt{\text{Hz}}},$$

where $C_0 = 19068$ cps, $C_1 = 16753$ cps, $\gamma = 28$ GHz and $\Gamma = 6.62$ MHz.

The sensitivity of AC magnetometry can similarly be derived using equation (4.6). In this case $\sigma_I = \sqrt{I_{avg}}$, and using $\delta B_{AC} = \delta y G_y$ we have $\sigma_{B_{AC}} \approx \frac{\sqrt{I_{avg}}}{I_{pk}\cos\left(\frac{\gamma B_{AC}}{\pi f_{osc}}\right)\frac{\gamma}{\pi f_{osc}}}$; however, we must be careful because the fluorescence $I_{avg/pk}$ is not continuous-wave as it is for DC magnetometry, but rather comes in pulses as the spin state is read out. If for a single pulse there are a number of photons $\epsilon_{avg/pk}$ that fluoresce, then in one second there will be $\epsilon_{avg/pk} f_{osc} = I_{avg/pk}$ photons incident on the photodiode. Thus we get the sensitivity for AC magnetometry,

$$\sigma_{B_{AC}} \approx \frac{\sqrt{\epsilon_{avg} f_{osc}}}{\epsilon_{pk}\gamma} \approx 0.92\frac{\mu\text{T}}{\sqrt{\text{Hz}}},$$

where $\epsilon_{avg} = 0.0199$/pulse , $\epsilon_{pk} = 0.0011$/pulse, and $f_{osc} = 41$ KHz.

To put these numbers in perspective, we can compare them to the current maximum achieved sensitivity of magnetic resonance force microscopy (MRFM), which is $2.3\frac{\text{nT}}{\sqrt{\text{Hz}}}$ [14]. We see that MRFM currently has better sensitivity, but note that further improvement in fluorescence collection efficiency is likely to enable NV magnetometry to reach comparable sensitivity [16]. Furthermore, MRFM is performed at cryogenic temperatures, and requires prohibitively long averaging times for most practical applications, whereas NV magnetometry can be performed at room temperature.

6 Methods

The ability to manipulate and measure a single spin is a remarkable scientific achievement, and is the culmination of extensive work going all the way back to the initial magnetic resonance experiments of Rabi, Purcell, Bloch, and Zavoiski in the 1940's. While NV centers have been studied in diamond since the 70's by Loubser and Van Wyk [18], it wasn't until 1997 that Gruber et al. [10] demonstrated that single NV centers could be seen through the use of a confocal fluorescence microscope, opening the door to a slough of new experiments. In the experiments by Yacoby et al. they use a similar

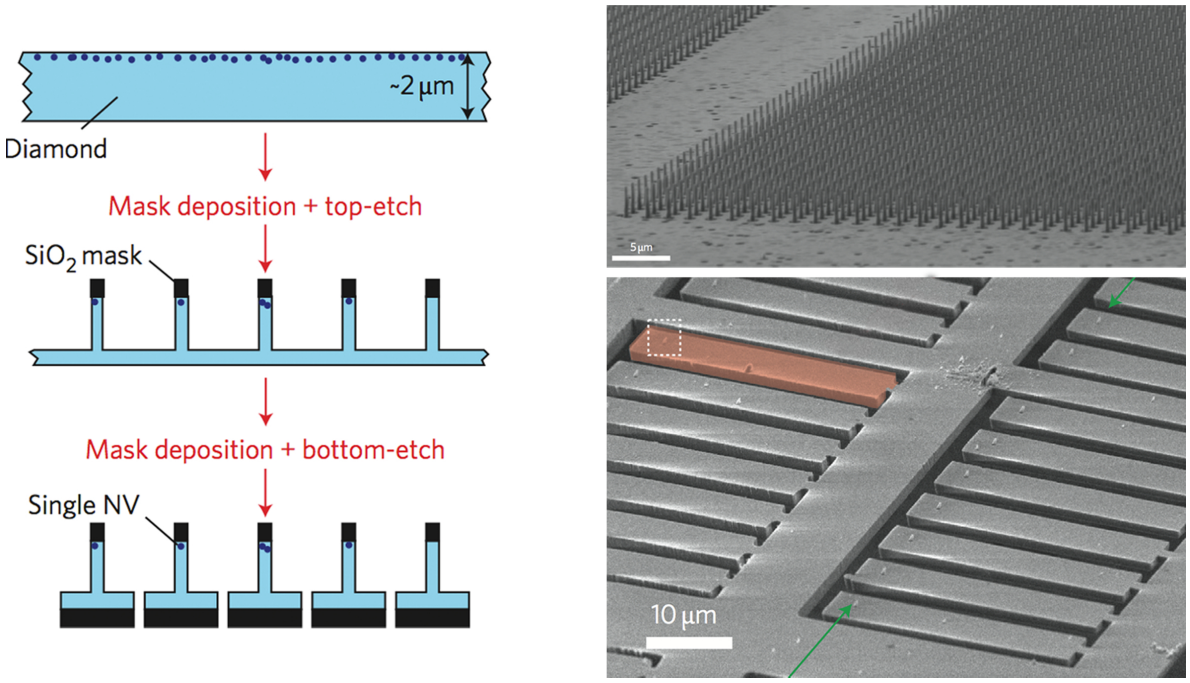

Figure 6.1: Left, schematic of the etching procedure. Starting from a thin diamond wafer, nitrogen is implanted shallowly beneath the surface, then annealed to form NV centers. The substrate is then masked and etched to create nano-pillars as pictured in the top right [13], which contain one NV center on average. Further etching can create a platform for a single nano pillar for scanning magnetometry as in figure (6.2)

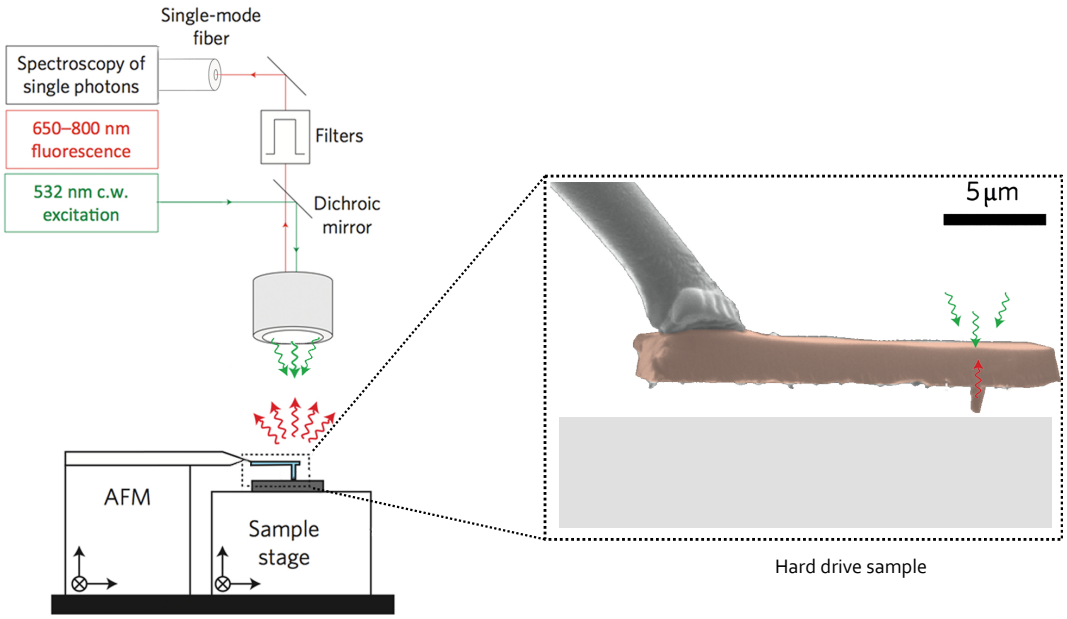

Figure 6.2: Left, confocal microscope setup and schematic of experiment. Right (zoom-in), an SEM image of a diamond nano pillar on a platform (in reddish false color) which is fused to a quartz tip, schematically shown scanning above the hard drive sample.

home-built confocal fluorescence microscope to illuminate their NV centers, but to isolate a single NV center without receiving fluorescence from any nearby NV centers required new techniques.

To isolate a single NV center, they shallowly implanted nitrogen atoms and then etched diamond nano-pillars. To do this they started with a film of diamond only a few microns thick, and accelerated nitrogen atoms towards the surface with an energy that implanted the nitrogen $\sim$ 10 nm below the surface. They then used e-beam lithography to create an etch mask that consisted of a row of disks diameters that corresponded to the average NV center spacing of $\sim$ 75 nm. The disks themselves were spaced 3 μm apart, larger than the beam size of the confocal microscope so that only one nano pillar would be illuminated at a time by the confocal microscope. Once the circles were etched, they were filled in with SiO_2 which was then lifted, leaving small cylinders of SiO_2 on an otherwise clean diamond surface. This was then subjected to reactive ion etching which leaves the SiO_2 intact and etches away the diamond straight down around it, leaving columns of diamond below the SiO_2 cylinders, which are the so-called 'nano-pillars.' Photon autocorrelation measurements were then performed on the

nano-pillars to verify that they did in fact contain just one NV center.

Since NV centers are not capable of emitting more than one photon at a time, one can deduce whether a single NV has been isolated by calculating the autocorrelation function

$$g^2(\tau) = \frac{\langle I(\tau)I(0)\rangle}{|\langle I\rangle|^2},$$

where the average fluorescence rate is given by $\langle I\rangle$, and $I(\tau)$ is the number of counts the detector receives at time $t = \tau$. We expect that $\langle I(\tau)I(0)\rangle$ for a single (Poisson) emitter will be zero for $\tau \to 0$, and it can be calculated [11, 12] that a single emitter can be deduced experimentally for $g(0) < \frac{1}{2}$, which is seen in figure 6.3.

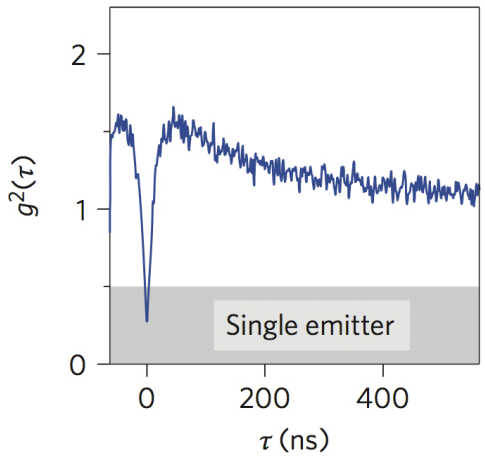

Figure 6.3: This second-order autocorrelation function shows that the emitter is in fact a single emitter because the $\tau = 0$ value is $< 1/2$ (in the grey).

To perform scanning magnetometry requires either the sample or the NV center to be scanned with respect to the other. In the experiments by Yacoby et al., both methods were used. To create an NV center that can be scanned over a sample, nano-pillars were created as previously discussed, which were then further etched from the back side of the diamond wafer to create individual platforms for each nano pillar, connected to the bulk diamond by just a very thin bridge (bottom right of figure 6.1). Under a scanning electron microscope (SEM) they used nanomanipulators to touch a quartz tip to one of the platforms that had a confirmed single-NV center, then deposited tungsten ions to fuse the two together. Finally the assembly was freed from the wafer by ion-milling the bridge with a focused ion beam (FIB).

The reverse method was also implemented, in which the NV center was kept fixed while a magnetic sample on a tip was scanned around it. A quartz tuning fork resonator was used for the oscillator in all experiment (DIGI-KEY, X801-ND), which is commercially used as a clock source. They separately

pulled quartz needles using a needle puller to make their tips with diameters of a few hundred nanometers, onto which they deposited a 25 nm layer of cobalt-iron which formed the dipole that was used as the magnetic sample. This was followed by a 5 nm layer of chrome as a protective capping. The oscillator was driven using a piezoelectric actuator, and the motion was read out electrically using the tuning fork's piezoelectric output. This contrasts to methods used in the related technique of MRFM, in which small magnetic particles are glued onto the end of $\sim 100\mu$m long cantilevers, and the motion is read out using interferometry.

7 Conclusion

In conclusion, the recent boom in research on NV centers is now bearing some very fruitful results. While the ultimate goals of using NV centers to create a scalable quantum computer, or to do single spin NMR on single molecules are still out of reach (although single spin NMR with ^{13}C has been demonstrated [18]), experiments such as those by Yacoby et al. demonstrate that it is possible to manipulate and measure the spin state of a single spin in a variety of ways, and to perform ultrasensitive magnetometry that could potentially be used for such applications. Other techniques such as MRFM have also measured single electrons in solid state systems, but these experiments have been at cryogenic temperatures and require exorbitant amounts of data collection time; the NV diamond spin state can be read out in nearly real time. While the NV center has only been used to measure magnetic samples with macroscopic numbers of electrons, it is foreseen by Yacoby that their future experiments will be able to measure the dipolar field of a single Bohr magneton within tens of seconds [6], which is the most exciting next step for the field.

Acknowledgements

I would like to thank Jeremy Cardellino and Richelle Teeling for useful conversations and their suggestions for improving the paper, as well as Zeke Johnston-Halperin for answering a few questions that I had regarding NV centers. I would also like to thank my family and friends for their support.

References

[1] John Walker. "Optical absorption and luminescence in diamond," *Rep. Prog. Phys.*, Vol. **42**, (1979)

[2] Zaritskii, I., Brutus, V., Vikhnin, V., and Vishnevskii, A. "Spin-lattice relaxation of a Jahn-Teller nitrogen center in diamond," *Sov. Phys. Solid State*, (1976)

[3] A. Lenef, S. W. Brown, D. A. Redman, and S. C. Rand. "Electronic structure of the N-V center in diamond: Experiments," *Phys. Rev. B* **53**, 13427–13440 (1996)

[4] S. Felton, et al. "Hyperfine interaction in the ground state of the negatively charged nitrogen vacancy center in diamond," *Phys. Rev. B* **79**, 075203 (2009)

[5] V. Acosta. "Optical Magnetometry with Nitrogen-Vacancy Centers in Diamond," Dissertation (2011)

[6] "Coherent, Mechanical Control of a Single Electronic Spin," *Nano Lett.* **12**, 3920-3924 (2012)

[7] "A robust scanning diamond sensor for nanoscale imaging with single nitrogen-vacancy centres," *Nature Nanotechnology* **7** 320 (2012)

[8] Loubser and Van Wyk, "Electron spin resonance in the study of diamond," Rep. Prog. Phys., Vol. **41**, 1978

[9] V.P. Markevich et al. "Defect reactions associated with the dissociation of the phosphorus–vacancy pair in silicon," *Physica B* 308–310 (2001)

[10] A. Gruber et al. "Scanning confocal optical microscopy and magnetic resonance on single defect centers," *Science*, **276**, 5321 (1997)

[11] L. Childress. "Coherent manipulation of single quantum systems in the solid state," Dissertation (2007)

[12] C. Kurtsiefer, S. Mayer, P. Zarda, and H. Weinfurter. Stable solid-state source of single photons. *Phys. Rev. Lett.*, 85:290, 2000

[13] Babinec, T. M., Hausmann, B. J. M., Khan, M., Zhang, Y., Loncar, M., Maze, J. R., & Hemmer, P. R. (March 01, 2010). A diamond nanowire single-photon source. *Nature Nanotechnology*, **5**, 3, 195-199.

[14] H. J. Mamin, T. H. Oosterkamp, M. Poggio, C. L. Degen, C. T. Rettner, and D. Rugar. *Nano Letters* **9**, 3020 (2009)

[15] Taylor, J. M., P. Cappellaro, L. Childress, L. Jiang, D. Budker, P. R. Hemmer, A. Yacoby, R. Walsworth, and M. D. Lukin. *Nature Physics* **7**, 3 (2008)

[16] J. Schwartz, S. Aloni, D. F. Ogletree, T. Schenkel. "Effects of low energy electron irradiation on formation of nitrogen-vacancy centers in single-crystal diamond," arXiv:1111.5055 (2012)

[17] S. Felton, A. M. Edmonds, and M. E. Newton. *Phys. Rev. B* **77**, 081201R 2008

[18] N. Zhao et al.. "Sensing single remote nuclear spins," *Nature Nanotechnology* **7**, 657–662 (2012)